Published in final edited form as:
Auton Neurosci. 2013 October ; 177(2): 199–210. doi:10.1016/j.autneu.2013.04.014.

High-fat diet and age-dependent effects on enteric glial cell populations of mouse small intestine

Chloe Stenkamp-Strahm[a], **Savannah Patterson**[a], **Jennifer Boren**[a], **Martin Gericke**[b], and **Onesmo Balemba**[a,*]

[a]University of Idaho, 875 Perimeter Drive, LSS 252, Moscow ID 83844, USA

[b]Institute for Anatomy, University of Leipzig, Liebigstraße 13, 04103 Leipzig, Germany

Abstract

Diabetes and obesity are increasing in prevalence at an alarming rate throughout the world. Autonomic diabetic neuropathy is evident in individuals that experience a long-standing diabetic disease state, and gastrointestinal (GI) dysmotility is thought to be the outcome of neuropathies within the enteric nervous system (ENS) of these patients. To date, an analysis of enteric glial cell population changes during diabetic symptoms has not been performed, and may bring insight into disease pathology and neuropathy, given glial cell implications in gastrointestinal and neuronal homeostasis. Diabetes and obesity were monitored in C57Bl/6J mice fed a 72% high-fat diet, and duodenal glial expression patterns were evaluated by immunohistochemistry and RT-PCR for S100β, Sox10 and GFAP proteins and transcripts, as well as transmission electron microscopy (TEM). The high-fat diet caused obesity, hyperglycemia and insulin resistance after 4 weeks. These changes were associated with a significant decline in the area density indices of mucosa-associated glial cell networks, evidenced by S100β staining at 8 and 20 weeks. All three markers and TEM showed that myenteric glial cells were unaffected by early and late disease periods. However, analysis of Sox10 transcript expression and immunoreactivity showed a diet independent, age-associated decline in glial cell populations. This is the first study showing that mucosal glia cell damage occurs during diabetic symptoms, suggesting that mucosal enteric glia injury may have a pathophysiological significance during this disease. Our results also provide support for age-associated changes in longitudinal studies of enteric glial cells.

Keywords

Enteric nervous system; Type 2 diabetes; S100β; Glial fibrillary acidic protein; Sox10; Enteric glial cell

Enteric glial cells (EGCs) reside in the gastrointestinal (GI) mucosal, submucosal and myenteric plexuses of the enteric nervous system (ENS), as well as muscle layers of the GI tract (Furness, 2006). They ensheath and are protective to neurons, and regulate substrate supply (Gabella, 1989; Cabarrocas et al., 2003; Furness, 2006). Further, EGCs play a role in

*Corresponding author at: University of Idaho, Department of Biological Sciences, 875 Perimeter Drive, LSS 252, Moscow ID 83844, USA. obalemba@uidaho.edu (O. Balemba).

GI neurotransmission, neuronal renewal, GI host defense, motility, secretion, and absorption (Savidge et al., 2007; Gulbransen and Sharkey, 2009, 2012). Regardless of these known properties, the pathophysiology of EGCs remains poorly understood.

Mucosal glia are implicated in intestinal epithelial barrier (EB) function by regulating tight junction protein expression (Savidge et al., 2007; Flamant et al., 2011), and influencing paracellular permeability and epithelial cell proliferation (Cabarrocas et al., 2003; Neunlist et al., 2007). EGCs also have an immunomodulatory role, as they can release cytokines and respond to their presence (Greene et al., 1988; von Boyen et al., 2004; Rühl, 2005). EGCs can modulate neuron phenotypes (Hökfelt, 1991; Rühl et al., 2001; Aubé et al., 2006), and release reduced glutathione or GDNF to activate NPY and anti-oxidant pathways protective to neurons (Anitha et al., 2006; von Boyen et al., 2006; Abdo et al., 2010, 2012). Loss of EGCs is therefore associated with neuronal degradation, and alterations in GI transit (Bush et al., 1998; Aubé et al., 2006). Although not previously assessed, these EGC roles may actively contribute to GI changes evident in type 2 diabetes (T2D).

T2D is a complex metabolic disease characterized by hyperglycemia and insulin resistance (Ohtsubo et al., 2011), but patients also exhibit symptoms of inflammation, dyslipidemia and disruption (Uysal et al., 1997; Dandona et al., 2004; Schinner et al., 2005; Ding et al., 2010). A negative secondary complication is autonomic neuropathy, often attributed to poor glucose regulation, oxidative stress, and dyslipidemia (Srinivasan et al., 2000; Watkins et al., 2000; Vincent et al., 2009; Katsilambros et al., 2011). In the ENS, nutrients are supplied by diffusion through connective tissues (Bagyánszki and Bódi, 2012), leaving plexuses exposed to circulating factors shown to cause nerve degeneration (von Boyen et al., 2006; Chandrasekharan and Srinivasan, 2007). Indeed, many diabetics have symptoms indicative of ENS pathology including constipation, diarrhea, and gastroparesis (Camilleri and Malagelada, 1984; Maleki et al., 2000).

Studies have demonstrated that enteric neuropathy contributes to these GI symptoms during type 1 diabetes (T1D). Neuropathies commonly impact nitrergic neurons, although remain heterogeneous among GI segments (He et al., 2001; Yoneda et al., 2001; Furlan et al., 2002; Bagyánszki and Bódi, 2012). T1D in rats leads to a decrease in GDNF and GFAP in colon, and a glia area reduction in ileum (Du et al., 2009; Liu et al., 2010; Pereira et al., 2011). Although studies concerning T1D are common, T2D is currently the predominant form of diabetes in society (Smyth and Heron, 2006). Further, neuronal analysis is usually sought in these contexts. EGCs can be implicated in the onset and maintenance of T2D and its negative secondary GI symptoms through EB maintenance, oxidative stress protection, immune modulation, and neuronal health influence. The results of a T2D EGC analysis will therefore add insight to secondary ENS symptoms and T2D disease pathology.

The purpose of this investigation was to analyze EGC populations during high-fat diet ingestion and T2D symptoms. We used an accelerated 72% high-fat diet mouse model (Cani et al., 2007) and performed an assessment of duodenal EGCs. The duodenum of the small intestine was chosen because it is implicated in glucose homeostasis, likely targeted during gastroparesis, and is removed during Roux-enY surgery to quell diabetes (Enck and Frieling, 1997; le Roux et al., 2011). Diabetic symptoms in mice were correlated to a reduction in

S100β density in the mucosa and submucosa, but not myenteric plexus. GFAP and Sox10 were also not affected in the myenteric plexus, but a Sox10 expression and cell count revealed age-associated declines in myenteric EGCs, and this was without ultrastructural alteration.

1. Materials and methods

1.1. Mice

C57Bl/6J mice were purchased from Jackson Laboratories (Bar Harbor, ME), housed in metal cages and kept on a 12:12 hour light cycle. Mice were fed with either a standard chow (SC) diet containing 6.2% fat (n = 13; Teklad Global 2018, Teklad Diets, Madison WI) or a high-fat (HF) diet containing 72% fat (n = 16; Modified DIO 70% kcal fat diet with 2% additional corn oil, TestDiet, Richmond, IN) ad libitum for 8 and 20 week time periods. These ingestion periods correlated to an age of 4.5 months (8 week duration) and 7.5 months (20 week duration). During the light cycle, mice were anesthetized with isoflurane and exsanguinated according to procedures approved by the University of Idaho Animal Care and Use Committee.

1.2. Obesity and type 2 diabetes assays

Mouse weights were monitored weekly. At euthanasia, epididymal fat pad tissues were excised and weighed.

Prior to euthanasia, mice were fasted for 6 h during onset of the light cycle. Briefly, blood was drawn by puncture of a submandibular vein and used to obtain blood glucose (BG) values with an Abbott AlphaTrak glucometer (Abbott Park, IL). Following an intra-peritoneal injection of glucose solution (1 g/kg^{-1}), BG was evaluated at 30 and 60 minute time points.

On the day of euthanasia, mice were fasted for 4 h during the light cycle and blood was drawn in a similar manner. Whole blood was used to obtain BG values, while serum was collected and stored at −80 °C. Insulin values were obtained using a Millipore ELISA kit (Billerica, MA). HOMA (homeostatic model assessment) was calculated as previously described (Matthews et al., 1985; Ding et al., 2010) to assess insulin resistance.

1.3. Tissue preparation

Duodenums from euthanized mice were immediately removed and placed in ice-chilled HEPES buffer (mmol L^{-1}: NaCl 134; KCl 6; $CaCl_2$ 2; $MgCl_2$ 1; HEPES 10; Glucose 10) for whole-mount longitudinal muscle myenteric plexus (LMMP) preparations, Krebs' solution for RNA extraction preparations (mmol L^{-1}: NaCl 121; KCl 5.9; $CaCl_2$ 2.5; $MgCl_2$ 1.2; $NaHCO_3$ 25; NaH_2PO_4 1.2; Glucose 8; aerated with 95% O_2/5% CO_2) or in the prepared fixatives described below. Unless otherwise specified all reagents and chemicals were purchased from Sigma-Aldrich (St Louis, MO).

1.4. Cryostat sections

A small duodenal segment (1.0 cm) was placed in 4% paraformaldehyde (PFA) with 0.2% picric acid and kept overnight at 4 °C. Tissues were washed three times in 0.1 M sodium phosphate buffer (PBS; 0.1 M PO_4, pH 7.4). Tissues were kept on a rotator at 4 °C and placed in 30%w/v sucrose solution, 1:1 30% w/v sucrose solution with O.C.T. (Sakura FineTek, Torrance, CA) each for 24 h on consecutive days. Tissues were embedded in O.C.T. medium and stored at−80 °C. 10 μm transverse sections were cut using a microtome.

1.5. Transmission electron microscopy tissue

A small duodenum segment (0.5 cm) was cut along the mesenteric border, pinned flat and fixed in 2.5% glutaraldehyde with 4% PFA (Electron Microscopy Sciences, Hatfield, PA). Tissues were washed three times in 0.1 M PBS, dehydrated in graded alcohol and stained with OsO_4 and uranyl acetate. After embedding in Durcupan Fluka resin and polymerization for 48 h at 56 °C, blocks were trimmed and ultrathin sections of 55 nm were prepared for use on an ultra-microtome. Sections were collected on Formvar-coated single-slot grids and stained by incubating in lead citrate. Cellular edema, swelling, rarefication/degeneration of mitochondria, and alteration in basement membranes have previously been defined as ultrastructural injury characteristics of EGCs (Schneider et al., 2010). These were evaluated in SC and HF mice using images containing 10–30 myenteric plexus nerve fibers, focusing on an analysis of glial cells with visible nuclei (n = 3–4, 2 images each, both time points). This was done using a Zeiss SIGMA electronmicroscope (Zeiss, Germany).

1.6. Longitudinal muscle myenteric plexus preparations (LMMP)

Duodenal segments (1.0 cm) were cut along the mesenteric border, pinned and stretched mucosa side-up in sylgard (Dow Corning, Midland, MI) lined glass dishes, and fixed in 4% PFA/0.2% picric acid overnight at 4 °C. Segments were washed three times in 0.1 M PBS. Mucosal, submucosal and circular muscle fibers were carefully removed using microdissection tools under stereomicroscopy to expose LMMP. LMMP tissue preparations were stored at 4 °C in 0.1 M sodium phosphate buffer containing 0.01 M NaN_3.

1.7. Dissection of muscularis externa preparations for Real-Time PCR

Duodenal segments (2.0 cm) were maintained in aerated (95% O_2, 5% CO_2) Kreb's solution throughout dissection. Tissues were pinned in sylgard-lined dishes and mucosa and submucosal layers were carefully removed, leaving muscularis externa and myenteric plexus intact. These tissue preparations were placed in RNA*later* (Quiagen, Valencia, CA) and kept at −20 °C.

1.8. RNA extraction, cDNA synthesis and real-time PCR

Tissues were homogenized and RNA isolated using an RNEasy mini kit (Quiagen, Valencia, CA). RNA yields were determined using a NanoDrop analyzer (ThermoScientific, Wilmington, DE). For cDNA synthesis, 100 μg total RNA was converted using an oligo ($dT_{12–18}$) primer, dNTP mix, First Strand Buffer, DTT and Superscript II (Invitrogen, Grand Island NY). Real-time PCR was performed on S100β, GFAP, Sox10 and Ppia (peptidylprolyl isomerase A; a neuronal housekeeping gene (Pernot et al., 2010) genes using

prepared cDNA, 10 pmol of each forward and reverse primer, SYBR green master mix (Applied Biosystems, Warrington, UK) and RNAse-free H_2O in each reaction. All samples were run in triplicate, using an Applied Biosystems 7900HT Fast Real-Time PCR System (Life Technologies, Carlsbad, CA). Relative gene expression was determined using the 2−ΔΔ−CT method (Livak and Schmittgen, 2001). The following primers were used: Ppia: forward gcggcaggtccatctacg reverse gccatccagccattcagtc; S100β: forward gagcaaatgatgctccagaa reverse taagtgtggctgtgctcctc; GFAP: forward aacgttaagctagccctgga reverse ggatctggaggttggagaaa; and Sox10: forward accagtaccctcacctccac reverse gcttgcctagtgtcttgctg. Primers were created using Primer3Plus and ordered from Fisher Scientific (Pittsburgh, PA).

1.9. Immunohistochemistry (IHC)

EGCs possess a densely integrated array of intermediate filaments made up of glial fibrillary acidic protein (GFAP) (Furness, 2006). They also produce and secrete S100β, a small neurotrophin protein, and Sox10, a transcription factor protein constitutively expressed in EGC nuclei (Hoff et al., 2008; Cirillo et al., 2011a,b). It is therefore possible to characterize EGCs using a chemical coding paradigm of GFAP, S100β and Sox10.

LMMP tissues were dual labeled with HuC/HuD and either Sox10 or GFAP primary antibodies. Full thickness sections were stained with S100β alone. Antibodies and dilutions used are presented in Table 1. All tissue washing and incubation steps were done on a multi-purpose rotator at room temperature. LMMP tissue preparations were washed three times for 20 min each in 0.1 M PBS containing 0.5% Triton X-100 (washing buffer). For detection of mouse antibodies on mouse tissue, a Vector M.O.M. Immunodetection Kit was used according to manufacturer's instructions (Vector Labs, Burlingame, CA). Tissues were incubated for one hour in washing buffer containing 5% normal donkey serum (NDS; Jackson ImmunoResearch, West Grove, PA). Primary antibodies were prepared in NDS. Tissues were incubated in primary antibody solution for 18–24 h, rinsed in washing buffer three times for 20 min each and incubated in secondary antibodies for 3 h. Tissues were washed and mounted on slides using VectaShield Mounting Medium (Vector Labs, Burlingame, CA).

For S100β staining in full thickness tissues the same procedure was employed, but 5% normal goat serum (NGS) was used in lieu of NDS (Jackson ImmunoResearch, West Grove, PA), washing steps were 5 min in duration, and a biotinylated secondary antibody with streptavidin Cy3 dye was employed to visualize staining.

To ensure nucleated cell localization, colocalization of DAPI for Sox10 and HuCD stained tissues was performed. Primary and secondary antibody negative control staining was performed for all markers used.

1.10. Morphometric analysis of EGC density indices

Tissues were photographed using a Nikon Eclipse Fluorescent microscope with a 20× non-oil objective lens (Nikon, Melville, NY) and analyzed using Metamorph2 software (Molecular Devices, Sunnyvale, CA). For LMMP tissues dual labeled with HuC/HuD and either GFAP or Sox10, at least 15 randomly selected ganglia were photographed using a

TRITC and FITC filter. Images were merged, and ganglionic area was measured after defining ganglionic borders based on the width of stained HuC/HuD neurons as previously described (Hoff et al., 2008). GFAP image thresholds were manually adjusted in a blinded fashion to allow software to select only stained segments within the ganglia, and this area was measured. For Sox10 images, individual Sox10 stained cells within ganglia were manually counted. It has been demonstrated that in order to overcome the effects of stretch and shrinkage during LMMP preparation, an estimation of surface area and absolute number of cells per area is best accomplished using ganglionic size as a reference, as ganglia are not thought to be affected by stretch (Karaosmanoglu et al., 1996). Therefore, estimations of the area of EGCs (GFAP stained cells) and absolute numbers of EGCs (Sox10 stained cells) were calculated based on ganglionic area (density index; GFAP) and Sox10 immunostained cells/ganglionic area, respectively.

For S100β analysis, four full thickness images per mouse were taken using the 20× objective. A tracing tool was used to trace and define regions of interest (mucosal, submucosal, and muscularis externa) in order to estimate total tissue area. Regions of interest were then manually thresholded in a blinded fashion to allow software to detect only the area of stained regions. Calculations of density index (stained area/total tissue area) were generated.

For demonstration of glia in LMMP, images of Sox10 and GFAP were acquired using an Olympus Fluoview confocal multiphoton microscope with a 60× oil objective and FluoView ASW acquisition software (Olympus, Center Valley, PA).

1.11. Statistical analysis

Statistical analyses were performed using GraphPad Prism 5 software (GraphPad Software Inc., La Jolla, CA). An unpaired Student's *t*-test was used to compare means of SC and HF mice, and in cases of multiple comparisons a repeated measures ANOVA with Bonferroni post-hoc test was utilized. Significance was determined as $P < 0.05$, and values are expressed as mean ± standard error of the mean. A mixed linear model was used to analyze ΔCT real-time PCR values (target gene CT-reference gene CT) of HF mice after normalization to SC using SAS 9.2 software (SAS Institute Inc., Cary, NC). For age effects, 20 week ΔCT animal values were normalized to 8 weeks. In figures, these values are expressed as mean fold change with standard deviation (according to the manufacturer's instructions).

2. Results

2.1. Obesity and T2D progression in 72% HF diet mice

A 72% HF diet fed ad libitum has been shown to initiate obesity and T2D in mice (Cani et al., 2007); however, this diet was only tested for up to 4 weeks. Therefore, we first evaluated disease progression over longer time points in order to select early and late disease time points for subsequent EGC analysis. Mice on the high-fat diet were euthanized after 8 and 20 weeks, and diabetic assays were also conducted with samples taken from live animals at 2 and 4 week time points.

To monitor obesity progression, the average weights of the mouse groups (HF or SC, fed ad libitum) were calculated each week. As healthy adult mice continued to grow throughout the study period, normal weight levels were assumed to be present in SC-fed mice, and mean group weights were compared each week by *t*-test to assess 'obesity/overweight onset'. Mean group weights became statistically different after 6 weeks (Fig. 1A, $P < 0.02$, $n = 3$). When evaluated as weight gained each week by group, mice on the HF diet experienced a statistically higher value of weight gained after 4 weeks (Fig. 1B, $P < 0.03$, $n = 3$). This indicates that the onset of obesity/overweight occurs at 4–6 weeks of diet ingestion. Meanwhile, the amount of weight gained as a proportion of initial body weight [initial weight (g)/total weight (g)] was assessed at all time points to verify weight gain was not influenced by initial animal weight. By 4 weeks HF mice have gained a greater proportion of their initial weight and the difference persisted at the 20 week time point (Fig. 1C, 4 weeks, $P < 0.0027$, $n = 16$; 8 weeks, $P < 0.001$, $n = 16$; 20 weeks, $P < 0.001$, $n = 6–7$).

At euthanasia epididymal fat pads were excised, weighed immediately, and expressed as a percentage of total mouse body weight. At 8 weeks, HF mice fat pads comprised a larger percentage of overall body mass when compared to SC, but these values were not different after 20 weeks (Fig. 1D, 8 weeks, $P < 0.001$, $n = 16$).

Compared to the SC group, HF mice experienced higher values of HOMA, indicating insulin resistance, after 4, 8 and 20 weeks of diet ingestion (Fig. 1E, 4 weeks, $P < 0.03$ $n = 5$; 8 weeks, $P < 0.03$, $n = 6–8$; 20 weeks, $P < 0.04$, $n = 5–6$). After 4 weeks mice on a HF diet had become glucose intolerant, as indicated by larger area under curve (AUC) values during fasting glucose challenge (Fig. 1F, 4 weeks, $P < 0.01$, $n = 4$). At 8 and 20 weeks the significant increase in AUC persisted (Fig. 1F, 8 weeks, $P < 0.01$, $n = 9–13$; 20 weeks, $P < 0.05$, $n = 5–6$) between SC and HF groups. Based on these findings that obesity and T2D symptoms are initiated by 4 weeks, we selected 8 week and 20 week time points (early and late stage disease, respectively) to use for EGC analysis, as circulating components correlated to neuropathy have effects based on continuing exposure (Papanas and Ziegler, 2012).

2.2. S100β glial cell density is reduced by HF diet in the mucosal and submucosal plexuses, but not in myenteric ganglia

S100β is a calcium binding protein expressed by EGCs (Ferri et al., 1982). Its cytoplasmic staining allows for optimal detection and quantification in full thickness tissue sections (Fig. 2A–D). Analysis of tissue areas (mucosa, submucosa, myenteric plexus) showed no significant difference in sizes between mice analyzed based on diet or age (data not shown). Compared to that of SC mice, EGC density index in the mucosal layer of HF mice was reduced at 8 and 20 weeks (Fig. 2E, 8 weeks, $P < 0.02$, $n = 6$; 20 weeks, $P < 0.0002$, $n = 5$). HF mice showed no decline in EGC density index in the submucosa after 8 weeks, but the density index was reduced at 20 weeks (Fig. 2F, 8 weeks, $n = 5$; 20 weeks, $P < 0.007$, $n = 6–7$). In the myenteric plexus, no EGC density index decline was detected at either time-point (Fig. 2G, 8 weeks, $n = 5–6$; 20 weeks, $n = 6–7$). Furthermore, neither the submucosal nor myenteric plexuses exhibited an age-dependent alteration (Fig. 2F and G, respectively). No difference in myenteric S100β transcript was detected between SC and HF mice at either

time point (Fig. 2H, 8 weeks, n = 4; 20 weeks, n = 6), and an age-wise analysis did not reveal a difference in S100β RNA levels at 20 compared to 8 weeks (Fig. 2I, n = 4).

2.3. HF diet ingestion does not alter GFAP expression in myenteric EGCs

Glial fibrillary acidic protein (GFAP) is also expressed by EGCs and comprises an array of densely packed intermediate filaments (Aubé et al., 2006; Furness, 2006; Hoff et al., 2008). GFAP and the pan neuronal marker HuC/HuD were used to label glia and neurons, respectively, in LMMP preparations (Fig. 3A–L). GFAP area indices were not different in mice based on diet or age (Fig. 3M, 8 weeks, n = 6–7; 20 weeks, n = 5). Consistent with the immunohistochemistry findings, RT-PCR analysis failed to detect differences in GFAP transcript levels based on the diet (Fig. 3N, 8 weeks n = 4; 20 weeks, n = 6) or age (Fig. 3O, n = 4).

2.4. Sox10 LMMP mRNA expression and number of stained cells declines with age, not HF diet ingestion

Sox10 is a transcription factor expressed by undifferentiated enteric crest-derived cells during development, and fully differentiated glial cells in adult mice (Young et al., 2003). Sox10 is the most consistent EGC marker, and its nuclear localization facilitates quantification of populations (Rühl et al., 2001). A combination of Sox10 and HuC/HuD antibodies were used to label glia and neurons, respectively, in LMMP preparations (Fig. 4A–L). The Sox10-labeled myenteric glial cell population did not differ between SC and HF mice at either the 8 or 20 time points (Fig. 4M, 8 weeks, n = 6–7; 20 weeks, n = 5). However, the number of glia declined from the 8 to 20 week points in both the SC-fed mice (Fig. 4M, $P < 0.03$, n = 5–7) and the mice on the HF diet (Fig. 4M, $P < 0.0029$, n = 5–7). Consistent with these findings, Sox10 mRNA expression was not influenced by high-fat diet (Fig. 4N, n = 4) but declined with age (Fig. 4O, $P < 0.05$, n = 4).

2.5. TEM analysis illustrates lack of diet and age-associated structural abnormalities in myenteric EGCs

Ultrastructural analysis by TEM revealed healthy (normal) EGCs surrounding nerve fibers in interganglionic connectives and muscularis nerve strands of SC (Fig. 5A, C) and HF (B, D) mice. Although nerve fibers (NF) within the mesaxon of EGCs already displayed axonal swelling and loss of neurofilaments/neurotubuli in HF mice (Fig. 5B, D, D4), these EGCs displayed no signs of apoptosis such as karyorrhexis or karyopyknosis. Further, nuclear membranes of HF mice showed no signs of rupture (Fig. 5D1), mitochondria lacked signs of swelling, rarefication and degeneration (Fig. 5D2), and basement membranes lacked any sign of thickening (Fig. 5D3). Surrounding muscle cells (MC) also exhibited normal morphology in chow and HF fed mice.

3. Discussion

Neuropathies thought to be due to hyperglycemia, dyslipidemia and metabolic syndrome occur in pre-diabetic and T2D individuals (Yamagishi and Imaizumi, 2005; Papanas and Ziegler, 2012). While peripheral diabetic neuropathy has been extensively studied in limb extremities and retina, ENS changes are less understood. The purpose of this investigation

was to determine how a HF diet and subsequent T2D symptoms correlate with small intestine enteric glial cell population changes in the mouse. The main findings indicate that a 72% HF diet causes obesity, hyperglycemia and insulin resistance beginning at 4 weeks. In this model, there is a reduction in the area density of glial cells in the duodenal mucosa, but the density and ultrastructure of EGCs in the myenteric plexus remain unaltered. In contrast, an age-dependent decline in the number of Sox10 expressing enteric glia occurs in the myenteric plexus, and this is independent of diet or disease state.

72% HF diet ingestion caused glucose intolerance and insulin resistance in mice after 4 weeks, which is consistent with previous findings using a hyperinsulinemic clamp and plasma glucose values (Cani et al., 2007). Body adiposity was estimated in the current study using a ratio of epididymal fat pad mass to that of the entire body, and we detected an increase in HF mice at 8 weeks and a normalization to control at 20 weeks. We hypothesize that the normalization of epididymal fat pad mass is due to increased fat deposition in sites other than these, as HF mice contain much larger visible levels of adipose tissue at 20 weeks in the mesentery and subcutaneous regions, compared to SC (Stenkamp–Strahm, personal observation). Meanwhile, as SC mice mature they deposit fat in epididymal areas initially, increasing this ratio and perhaps overestimating their level of body adiposity. Regardless, 8 weeks of diet ingestion was considered as an early state of diabetic insulin resistance and glucose intolerance with overweight/obesity present, while 20 weeks was considered a prolonged disease state.

Our S100β analysis suggests that from 8 weeks onward, EGC injury during HF diet ingestion is occurring primarily in the mucosa. Although the mechanism leading to this decline in density is not understood, it merits further study since potential consequences for mucosal EGC damage are extensive. Mucosal EGCs can aid in the mucosal healing process (Van Landeghem et al., 2011), facilitate epithelial ion transport (MacEachern et al., 2011) and impact epithelial cell size and growth (Neunlist et al., 2007). Maintaining these functions would be highly beneficial during T2D as intestinal epithelial barrier disruption is characteristic of the disease state (Cani and Delzenne, 2009), although the disruption itself may also be aiding in these EGC population effects.

Also, it is possible that the absorption of large amounts of fatty acids and endotoxins (Srinivasan et al., 2000; Cani et al., 2007; Cani and Delzenne, 2009; Vincent et al., 2009), and/or increased oxidative stress and low-grade inflammation (Ding et al., 2010; Cirillo et al., 2011a,b) in the GI tract are among the causes for the mucosal EGC changes reported here. Further, the observation of a reduced EGC density index in the submucosa at 20 weeks suggests that an even longer-standing disease state may boast damage to EGCs of the major ganglionated plexuses. A full-thickness analysis of GFAP and Sox10 markers to potentially bolster these conclusions was not accomplished due to an inability of these markers to adequately label intramucosal EGCs, and cause nonspecific staining due to submucosal glands of Brünner. Interestingly, our findings contrast with an up-regulation of S100β seen during GI inflammatory disease pathology (Cirillo et al., 2011a,b), which parallels our model since GI inflammation has been reported in mice with HF diet-induced T2D (Ding et al., 2010). However, several other lines of evidence support our findings. It has been shown that serum S100β concentrations in type 2 diabetic, but not type 1 diabetic humans are

significantly lower than those found in healthy controls (Hovsepyan et al., 2004). In addition, experiments using cultured astrocytes have shown that chronic elevated glucose and beta-hydroxy-butyrate levels affect astrocyte activity by reducing extracellular secretion of S100β (Leite et al., 2004; Nardin et al., 2007). When taken together with the present findings, a reduction in S100β may be the result of hyperglycemia and dyslipidemia. To effectively tie these changes to HF diet ingestion and diabetic symptoms, our findings suggest the need to identify the molecules or structural GI changes that ultimately cause inhibition of this protein, potentially damaging EGCs.

In this study a Sox10 analysis revealed an age, but not diet or disease state-dependent, decline of EGCs in the LMMP of mouse duodenum from 4.5 months of age (8 week mice group) to 7.5 months of age (20 week mice group). Based on classification of mice being ‘mature adult’ at 3–6 months, ‘middle-aged’ at 10–14 months and ‘old’ at 18–24 months (The Mouse in Biomedical Research, 2006), our data show that this decline occurs in adult mouse duodenum. It is possible that these results are due to a decline in Sox10 stained non-differentiated neural-crest progenitor cells, as these have been seen to express Sox10 and decline with age in adult animals (Paratore et al., 2001). Our results also have only taken into account ganglionic glial cells, and it is possible that extra-ganglionic cells, if included, would impact these outcomes. Regardless of these implications, our results of S100β LMMP density index reveal trends similar to those seen with Sox10, and would potentially become significant given a larger study cohort of mice (see Fig. 2G, SC mice, $P = 0.08$, $n = 5–7$). Although looking at EGC populations in healthy versus diseased mice was the ultimate goal of this work, this secondary finding suggests a need to know EGC population levels prior to any diet ingestion, specifically because EGC decline may be associated with loss of enteric neurons over time (Phillips et al., 2004). Indeed, El-Salhy and colleagues (El-Salhy et al., 1999) demonstrated a 50– 60% decline in the number of myenteric neurons of mouse duodenum between 3 and 12 months of age. Also, the number of myenteric neurons in guinea pig small intestine undergoes a decline between 3 and 30 months of age (Gabella, 1981). This loss of neurons may equate to functional change, and previous studies have shown a loss of EGCs alone causing the same conclusion (Bassotti et al., 2005, 2006). Since functional studies were not the goal of this work, we cannot conclusively rule-out or infer functional changes to be present in our mice based on these indications. A TEM analysis of cells in muscularis externa showed that the ultrastructural features of EGCs appeared normal in the HF diet fed mice at both time points, regardless of the degenerative state of nerve fibers associated with them (unpublished results). It is therefore unknown whether the Sox10 loss we see is mediated through apoptosis or another mechanism. Interestingly, a recent paper by Baudry et al. (2012) found Sox10 labeled cells to increase in antrum and remain unaltered in jejunum after 12 weeks of 36% HF diet ingestion. The mice used in this study were 5 weeks of age at the beginning of diet ingestion and showed less advanced metabolic symptoms than mice in the current study, showing that the interplay of animal development, method of disease induction, and selection of GI tissue for study may alter the outcome of any longitudinal EGC analysis. Regardless, our results coupled with these implications give justification to probe the mechanisms behind age-associated EGC population changes.

Myenteric plexus density index of GFAP and GFAP expression did not change based on age or diet-induced obesity and T2D. For our conclusions of cell loss based on Sox10 data to be

accurate, we must assume that GFAP expression increased in remaining glial cells. Although we did not detect a change in staining density in aged mice, it is possible an increased expression is still occurring, as it is only possible to compare stained areas of the tissue, and not intensity levels. T2D and obesity are both states of chronic, systemic low-grade inflammation (Dandona et al., 2004), and intestinal inflammation has been shown to precede and correlate to onset of disease (Ding et al., 2010). GFAP expression increases during exposure to pro-inflammatory mediators in vitro (von Boyen et al., 2004) while in vivo studies done with type 1 diabetic mice have showed decreases in CNS (Coleman et al., 2004) and colonic (Liu et al., 2010) levels of GFAP. This, however, does not allow us to infer why there is lack of age-associated decline in GFAP stained area in LMMP, assuming there are less cells given our Sox10 results. Although this is the first study to analyze GFAP expression in duodenum, a previous study detected GFAP non-labeled EGCs in rat colon tissues and cultured cells (62). Importantly, the cytoplasmic staining patterns of GFAP require a density analysis that is not perfectly objective, and may lack sensitivity required to deduce differences between test groups. Due to all of these confounding factors, a more thorough analysis of this protein will need to be completed to fully understand its regulation within a context of obesity and T2D symptoms.

In its entirety, this study suggests that damage to EGCs of the small intestine mucosa is evident in mice with obesity and T2D symptoms, and may play a role in the larger enteric neuropathies associated with T2D. Age-related myenteric plexus decline of EGCs is also evident, and may be correlated to a commonly seen age-wise ENS neuron loss. As changes in EGC population levels retain the capacity to instigate functional GI changes, future longitudinal studies of the healthy and pathology-ridden ENS ought to consider these conclusions.

Acknowledgments

Funding

This study was funded by The University of Idaho WWAMI Medical Education Program, Idaho INBRE (NIH Grant Nos. P20 RR016454 and P20 GM103408) and a University of Idaho Starter-Up fund.

The authors would like to thank Dr. Peter Fuerst for guidance and editorial comment. We would also like to thank Joe Schmalz and Adam Kappmeyer for work on staining analysis, as well as Celeste Brown for help with statistics.

References

Abdo H, Derkinderen P, Gomes P, Chevalier J, Aubert P, Masson D, et al. Enteric glial cells protect neurons from oxidative stress in part via reduced glutathione. FASEB J. 2010; 24:1082–1094. [PubMed: 19906678]

Abdo H, Mahé MM, Derkinderen P, Bach-Ngohou K, Neunlist M, Lardeux B, et al. The omega-6 derivative 15d-PGJ2 is involved in neuroprotection by enteric glial cells against oxidative stress. J. Physiol. 2012; 590:2739–2750. [PubMed: 22473776]

Anitha M, Chandrasekharan B, Salgado JR, Grouzmann E, Mwangi S, Sitaraman SV. Glial-derived neurotrophic factor modulates enteric neuronal survival and proliferation through neuropeptide Y. Gastroenterology. 2006; 131:1164–1178. [PubMed: 17030186]

Aubé A-C, Cabarrocas J, Bauer J, Philippe D, Aubert P, Doulay F, et al. Changes in enteric neurone phenotype and intestinal functions in a transgenic mouse model of enteric glia disruption. Gut. 2006; 55:630–637. [PubMed: 16236773]

Bagyánszki M, Bódi N. Diabetes-related alterations in the enteric nervous system and its microenvironment. World. J. Diabetes. 2012; 3:80–93. [PubMed: 22645637]

Bassotti G, Battaglia E, Bellone G, Dughera L, Fisogni S, Zambelli C, et al. Interstitial cells of Cajal, enteric nerves, and glial cells in colonic diverticular disease. J. Clin. Pathol. 2005; 58:973–977. [PubMed: 16126881]

Bassotti G, Villanacci V, Maurer CA, Fisogni S, Di Fabio F, Cadei M, et al. The role of glial cells and apoptosis of enteric neurones in the neuropathology of intractable slow transit constipation. Gut. 2006; 55:41–46. [PubMed: 16041063]

Baudry C, Reichardt F, Marchix J, Bado A, Schemann M, des Varannes SB, et al. Diet-induced obesity has neuroprotective effects in murine gastric enteric nervous system: involvement of leptin and glial cell line-derived neurotrophic factor. J. Physiol. 2012; 2012(590):533–544. [PubMed: 22124147]

Bush TG, Savidge TC, Freeman TC, Cox HJ, Campbell EA, Mucke L, et al. Fulminant jejuno-ileitis following ablation of enteric glia in adult transgenic mice. Cell. 1998; 93:189–201. [PubMed: 9568712]

Cabarrocas J, Savidge TC, Liblau RS. Role of enteric glial cells in inflammatory bowel disease. Glia. 2003; 41:81–93. [PubMed: 12465048]

Camilleri M, Malagelada JR. Abnormal intestinal motility in diabetics with the gastroparesis syndrome. Eur. J. Clin. Invest. 1984; 14:420–427. [PubMed: 6441717]

Cani PD, Delzenne NM. The role of the gut microbiota in energy metabolism and metabolic disease. Curr. Pharm. Des. 2009; 15:1546–1558. [PubMed: 19442172]

Cani PD, Amar J, Iglesias MA, Poggi M, Knauf C, Bastelica D, et al. Metabolic endotoxemia initiates obesity and insulin resistance. Diabetes. 2007; 56:1761–1772. [PubMed: 17456850]

Chandrasekharan B, Srinivasan S. Diabetes and the enteric nervous system. Neurogastroenterol. Motil. 2007; 19:951–960. [PubMed: 17971027]

Cirillo C, Sarnelli G, Turco F, Mango A, Grosso M, Aprea G, et al. Proinflammatory stimuli activates human-derived enteroglial cells and induces autocrine nitric oxide production. Neurogastroenterol. Motil. 2011; 23:372–382.

Cirillo C, Sarnelli G, Esposito G, Turco F, Steardo L, Cuomo R. S100B protein in the gut: the evidence for enteroglial-sustained intestinal inflammation. World. J. Gastroenterol. 2011; 17:1261–1266. [PubMed: 21455324]

Coleman E, Judd R, Hoe L, Dennis J, Posner P. Effects of diabetes mellitus on astrocyte GFAP and glutamate transporters in the CNS. Glia. 2004; 48:166–178. [PubMed: 15378652]

Dandona P, Aljada A, Bandyopadhyay A. Inflammation: the link between insulin resistance, obesity and diabetes. Trends Immunol. 2004; 25:4–7. [PubMed: 14698276]

Ding S, Chi MM, Scull BP, Rigby R, Schwerbrock NMJ, Magness S, et al. High-fat diet: bacteria interactions promote intestinal inflammation which precedes and correlates with obesity and insulin resistance in mouse. PLoS One. 2010; 5:e12191. [PubMed: 20808947]

Du F, Wang L, Qian W, Liu S. Loss of enteric neurons accompanied by decreased expression of GDNF and PI3K/Akt pathway in diabetic rats. Neurogastroenterol. Motil. 2009; 21:1229–e114. [PubMed: 19709371]

El-Salhy M, Sandström O, Holmlund F. Age-induced changes in the enteric nervous system in the mouse. Mech. Ageing Dev. 1999; 107:93–103. [PubMed: 10197791]

Enck P, Frieling T. Pathophysiology of diabetic gastroparesis. Diabetes. 1997; 46:S77–S81. [PubMed: 9285504]

Ferri GL, Probert L, Cocchia D, Michetti F, Marangos PJ, Polak JM. Evidence for the presence of S-100 protein in the glial component of the human enteric nervous system. Nature. 1982; 297:409–410. [PubMed: 7043279]

Flamant M, Aubert P, Rolli-Derkinderen M, Bourreille A, Neunlist MR, Mahé MM, et al. Enteric glia protect against *Shigella flexneri* invasion in intestinal epithelial cells: a role for S-nitrosoglutathione. Gut. 2011; 60:473–484. [PubMed: 21139062]

Furlan MM, Molinari SL, Miranda Neto MH. Morphoquantitative effects of acute diabetes on the myenteric neurons of the proximal colon of adult rats. Arq. Neuropsiquiatr. 2002; 60:576–581. [PubMed: 12244395]

Furness, JB. The Enteric Nervous System. Wiley-Blackwell; 2006. p. 288

Gabella G. Ultrastructure of the nerve plexuses of the mammalian intestine: the enteric glial cells. Neuroscience. 1981; 6:425–436. [PubMed: 7219723]

Gabella G. Fall in the number of myenteric neurons in aging guinea pigs. Gastroenterology. 1989; 96:1487–1493. [PubMed: 2714575]

Greene DA, Lattimer SA, Sima AA. Are disturbances of sorbitol, phosphoinositide, and Na^+-K^+-ATPase regulation involved in pathogenesis of diabetic neuropathy? Diabetes. 1988; 37:688–693. [PubMed: 2838351]

Gulbransen BD, Sharkey KA. Purinergic neuron-to-glia signaling in the enteric nervous system. Gastroenterology. 2009; 136:1349–1358. [PubMed: 19250649]

Gulbransen BD, Sharkey KA. Novel functional roles for enteric glia in the gastrointestinal tract. Nat. Rev. Gastroenterol. Hepatol. 2012; 9:625–632. [PubMed: 22890111]

He CL, Soffer EE, Ferris CD, Walsh RM, Szurszewski JH, Farrugia G. Loss of interstitial cells of cajal and inhibitory innervation in insulin-dependent diabetes. Gastroenterology. 2001; 121:427–434. [PubMed: 11487552]

Hoff S, Zeller F, von Weyhern CWH, Wegner M, Schemann M, Michel K, et al. Quantitative assessment of glial cells in the human and guinea pig enteric nervous system with an anti-Sox8/9/10 antibody. J. Comp. Neurol. 2008; 509:356–371. [PubMed: 18512230]

Hökfelt T. Neuropeptides in perspective: the last ten years. Neuron. 1991; 7:867–879. [PubMed: 1684901]

Hovsepyan MR, Haas MJ, Boyajyan AS, Guevorkyan AA, Mamikonyan AA, Myers SE, et al. Astrocytic and neuronal biochemical markers in the sera of subjects with diabetes mellitus. Neurosci. Lett. 2004; 369:224–227. [PubMed: 15464269]

Karaosmanoglu T, Aygun B, Wade PR, Gershon MD. Regional differences in the number of neurons in the myenteric plexus of the guinea pig small intestine and colon: an evaluation of markers used to count neurons. Anat. Rec. 1996; 244:470–480. [PubMed: 8694282]

Katsilambros NL, Boulton AJ, Tentolouris N, Kokkinos A, Liatis S. Autonomic neuropathy in diabetes mellitus and obesity: an update. Exp. Diabetes Res. 2011:607309. [PubMed: 22203830]

le Roux CW, Bueter M, Theis N, Werling M, Ashrafian H, Löwenstein C, Athanasiou T, Bloom SR, Spector AC, Olbers T, Lutz TA. Gastric bypass reduces fat intake and preference. Am. J. Physiol. Regul. Integr. Comp. Physiol. 2011; 301(4):R1057–R1066. [PubMed: 21734019]

Leite M, Frizzo JK, Nardin P, de Almeida LMV, Tramontina F, Gottfried C, et al. Beta-hydroxy-butyrate alters the extracellular content of S100B in astrocyte cultures. Brain Res. Bull. 2004; 64:139–143. [PubMed: 15342101]

Liu W, Yue W, Wu R. Effects of diabetes on expression of glial fibrillary acidic protein and neurotrophins in rat colon. Auton. Neurosci. 2010; 154:79–83. [PubMed: 20042376]

Livak KJ, Schmittgen TD. Analysis of relative gene expression data using real-time quantitative PCR and the 2(−Delta Delta C(T)) Method. Methods. 2001; 25:402–408. [PubMed: 11846609]

MacEachern SJ, Patel BA, McKay DM, Sharkey KA. Nitric oxide regulation of colonic epithelial ion transport: a novel role for enteric glia in the myenteric plexus. J. Physiol. 2011; 589:3333–3348. [PubMed: 21558161]

Maleki D, Locke GR, Camilleri M, Zinsmeister AR, Yawn BP, Leibson C, et al. Gastrointestinal tract symptoms among persons with diabetes mellitus in the community. Arch. Intern. Med. 2000; 160:2808–2816. [PubMed: 11025791]

Matthews DR, Hosker JP, Rudenski AS, Naylor BA, Treacher DF, Turner RC. Homeostasis model assessment: insulin resistance and beta-cell function from fasting plasma glucose and insulin concentrations in man. Diabetologia. 1985; 28:412–419. [PubMed: 3899825]

Nardin P, Tramontina F, Leite MC, Tramontina AC, Quincozes-Santos A, de Almeida LMV, et al. S100B content and secretion decrease in astrocytes cultured in high-glucose medium. Neurochem. Int. 2007; 50:774–782. [PubMed: 17350141]

Neunlist M, Aubert P, Bonnaud S, Van Landeghem L, Coron E, Wedel T, et al. Enteric glia inhibit intestinal epithelial cell proliferation partly through a TGF-beta1-dependent pathway. Am. J. Physiol. Gastrointest. Liver Physiol. 2007; 292:231–241.

Ohtsubo K, Chen MZ, Olefsky JM, Marth JD. Pathway to diabetes through attenuation of pancreatic beta cell glycosylation and glucose transport. Nat. Med. 2011; 17:1067–1075. [PubMed: 21841783]

Papanas, N.; Ziegler, D. Prediabetic neuropathy: does it exist?. Curr. Diab. Rep. 2012. http://dx.doi.org/10.1007/s11892-012-0278-3

Paratore C, Goerich DE, Suter U, Wegner M, Sommer L. Survival and glial fate acquisition of neural crest cells are regulated by an interplay between the transcription factor Sox10 and extrinsic combinatorial signaling. Development. 2001; 128:3949–3961. [PubMed: 11641219]

Pereira RVF, Tronchini EA, Tashima CM, Alves EPB, Lima MM, Zanoni JN. l-glutamine supplementation prevents myenteric neuron loss and has gliatrophic effects in the ileum of diabetic rats. Dig. Dis. Sci. 2011; 56:3507–3516. [PubMed: 21710226]

Pernot F, Dorandeu F, Beaup C, Peinnequin A. Selection of reference genes for real-time quantitative reverse transcription-polymerase chain reaction in hippocampal structure in a murine model of temporal lobe epilepsy with focal seizures. J. Neurosci. Res. 2010; 88:1000–1008. [PubMed: 19937810]

Phillips RJ, Hargrave SL, Rhodes BS, Zopf DA, Powley TL. Quantification of neurons in the myenteric plexus: an evaluation of putative pan-neuronal markers. J. Neurosci. Methods. 2004; 133:99–107. [PubMed: 14757350]

Rühl A. Glial cells in the gut. Neurogastroenterol. Motil. 2005; 17:777–790. [PubMed: 16336493]

Rühl A, Franzke S, Collins SM, Stremmel W. Interleukin-6 expression and regulation in rat enteric glial cells. Am. J. Physiol. Gastrointest. Liver Physiol. 2001; 280:1163–1171.

Savidge TC, Newman P, Pothoulakis C, Ruhl A, Neunlist M, Bourreille A, et al. Enteric glia regulate intestinal barrier function and inflammation via release of S-nitrosoglutathione. Gastroenterology. 2007; 132:1344–1358. [PubMed: 17408650]

Schinner S, Scherbaum WA, Bornstein SR, Barthel A. Molecular mechanisms of insulin resistance. Diabet. Med. 2005; 22:674–682. [PubMed: 15910615]

Schneider R, Welt K, Aust W, Kluge R, Löster H, Fitzl G. Cardiovascular autonomic neuropathy in spontaneously diabetic rats with and without application of EGb 761. Histol. Histopathol. 2010; 25:1581–1590. [PubMed: 20886438]

Smyth S, Heron A. Diabetes and obesity: the twin epidemics. Nat. Med. 2006; 12:75–80. [PubMed: 16397575]

Srinivasan S, Stevens M, Wiley JW. Diabetic peripheral neuropathy: evidence for apoptosis and associated mitochondrial dysfunction. Diabetes. 2000; 49:1932–1938. [PubMed: 11078462]

The Mouse in Biomedical Research. American College of Laboratory Animal Medicine. 2nd edition. Academic Press; 2006. p. 2192

Uysal KT, Wiesbrock SM, Marino MW, Hotamisligil GS. Protection from obesity-induced insulin resistance in mice lacking TNF-alpha function. Nature. 1997; 389:610–614. [PubMed: 9335502]

Van Landeghem L, Chevalier J, Mahé MM, Wedel T, Urvil P, Derkinderen P, et al. Enteric glia promote intestinal mucosal healing via activation of focal adhesion kinase and release of proEGF. Am. J. Physiol. Gastrointest. Liver Physiol. 2011; 300:976–987.

Vincent AM, Hayes JM, McLean LL, Vivekanandan-Giri A, Pennathur S, Feldman EL. Dyslipidemia-induced neuropathy in mice: the role of oxLDL/LOX-1. Diabetes. 2009; 58:2376–2385. [PubMed: 19592619]

von Boyen GBT, Steinkamp M, Reinshagen M, Schäfer K-H, Adler G, Kirsch J. Proinflammatory cytokines increase glial fibrillary acidic protein expression in enteric glia. Gut. 2004; 53:222–228. [PubMed: 14724154]

von Boyen GBT, Steinkamp M, Reinshagen M, Schäfer K-H, Adler G, Kirsch J. Nerve growth factor secretion in cultured enteric glia cells is modulated by proinflammatory cytokines. J. Neuroendocrinol. 2006; 18:820–825. [PubMed: 17026531]

Watkins CC, Sawa A, Jaffrey S, Blackshaw S, Barrow RK, Snyder SH, et al. Insulin restores neuronal nitric oxide synthase expression and function that is lost in diabetic gastropathy. J. Clin. Invest. 2000; 106:373–384. [PubMed: 10930440]

Yamagishi S, Imaizumi T. Diabetic vascular complications: pathophysiology, biochemical basis and potential therapeutic strategy. Curr. Pharm. Des. 2005; 11:2279–2299. [PubMed: 16022668]

Yoneda S, Kadowaki M, Kuramoto H, Fukui H, Takaki M. Enhanced colonic peristalsis by impairment of nitrergic enteric neurons in spontaneously diabetic rats. Auton. Neurosci. 2001; 92:65–71. [PubMed: 11570705]

Young HM, Bergner AJ, Müller T. Acquisition of neuronal and glial markers by neural crest-derived cells in the mouse intestine. J. Comp. Neurol. 2003; 456:1–11. [PubMed: 12508309]

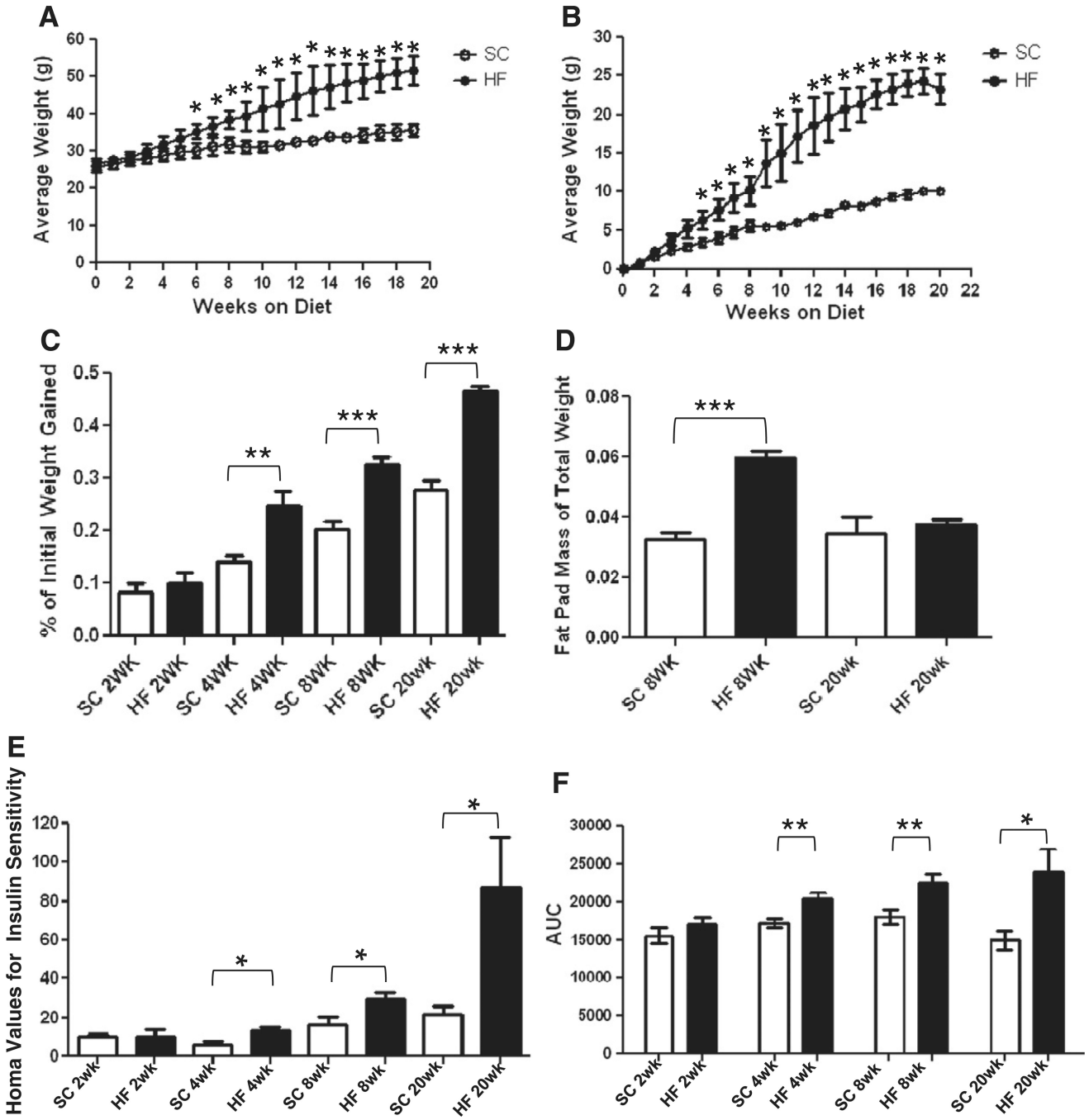

Fig. 1.

C57Bl/6 mice on a HF diet experience hallmarks of obesity and type 2 diabetes. After 6 weeks of HF diet ingestion, mice exhibited greater average weights than their SC counterparts (A; n = 3, *P < 0.05, unpaired *t*-test). At 4 weeks mice on a HF diet also experience greater total weight gain (B; n = 3, *P < 0.05, unpaired *t*-test) indicating the onset of obesity/overweight between 4 and 6 weeks. This is regardless of initial weight, shown by a greater proportion of initial body weight gain (C) at 4 (n = 16, **P < 0.01 unpaired *t*-test), 8 (n = 16, ***P < 0.001, unpaired *t*-test) and 20 weeks (n = 6–7). HF diet

mice had greater epididymal fat pad mass expressed as a percentage of total body weight (D) at 8 (n = 16, ***P < 0.001 unpaired *t*-test) but not 20 weeks of HF diet ingestion (n = 6–7). HOMA values for insulin resistance were higher in mice on a HF diet at 4, 8 and 20 week time-points (E; n = 5, **P < 0.01; n = 6–8, **P < 0.01; n = 5–6, *P < 0.05; all unpaired *t*-test). After generating a curve of blood glucose levels pre and post 1 g/kg^{-1} IP glucose injection, area-under-curve (AUC) values became greater in 4, 8 and 20 week mice (F; n = 4, *P < 0.05; n = 9–13, *P <0.05; n = 5–6, *P < 0.05; all unpaired *t*-test) indicating glucose intolerance.

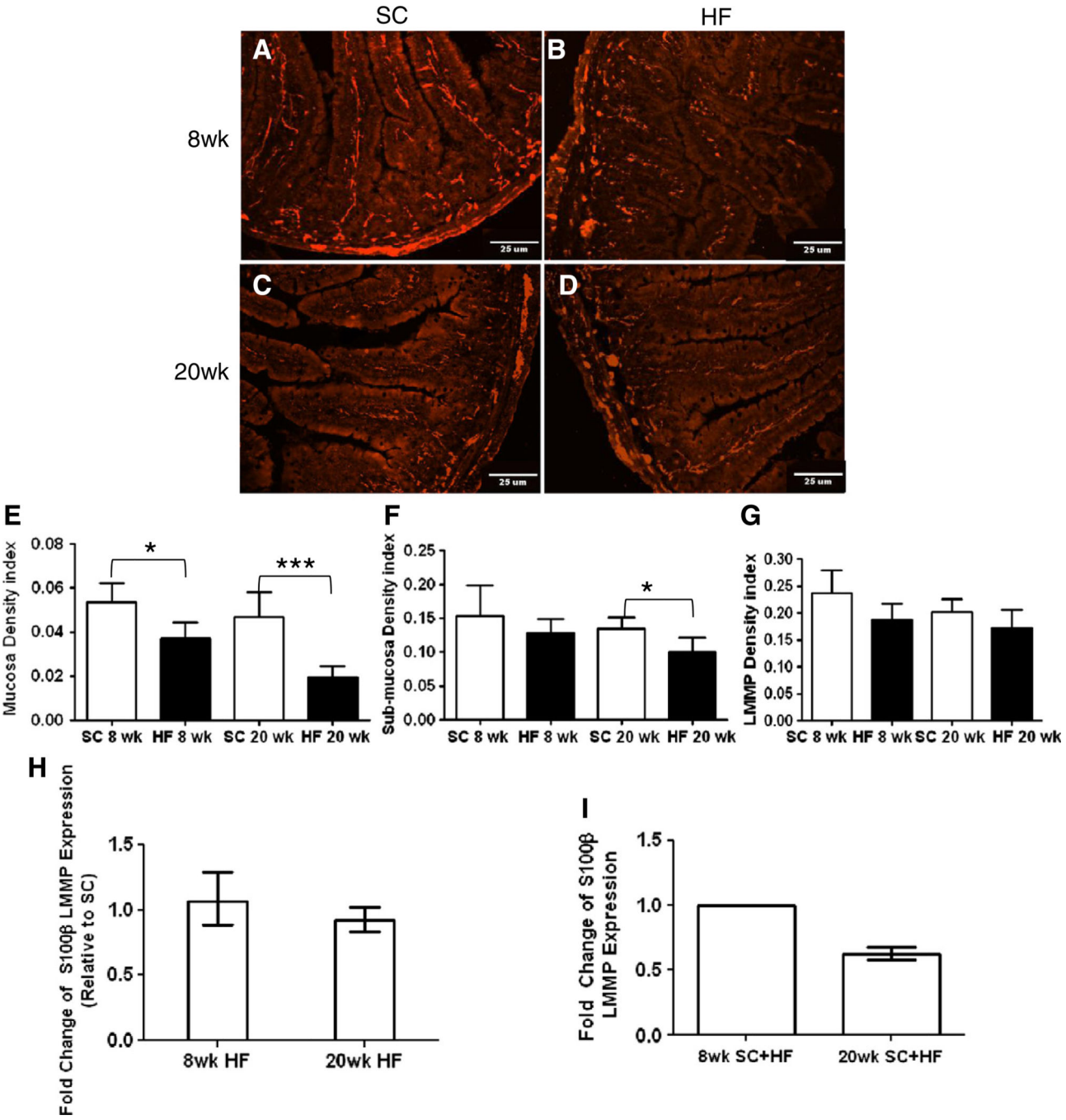

Fig. 2.

Effect of diet on S100β expression in mouse duodenum. 10 μmduodenum cryostat sections of SC (A, C) and HF (B, D) mice were stained with antibodies to S100β protein after 8 (A–B) and 20 weeks (C–D). Analysis of density indexes (stained area/total tissue area) in the mucosa showed a significant decline in HF diet mice after 8 and 20 weeks (E; 8 weeks, n = 5, *P < 0.05; 20 weeks, n = 6–7, ***P < 0.001; unpaired students *t*-test). EGC density index of sub-mucosal plexus showed a decline due to high-fat diet only after 20 weeks (F; 8 weeks, n = 5; 20 weeks, n = 6–7, *P < 0.05; unpaired students *t*-test) while density in

LMMP remained unchanged (G; SC n = 5; HF n = 6–7). RT-PCR expression levels of S100β in LMMP of HF diet fed mice was not significantly different than SC (H; 8 weeks n = 4; 20 weeks, n = 6), and was also not significantly different based on mouse age (I; n = 4).

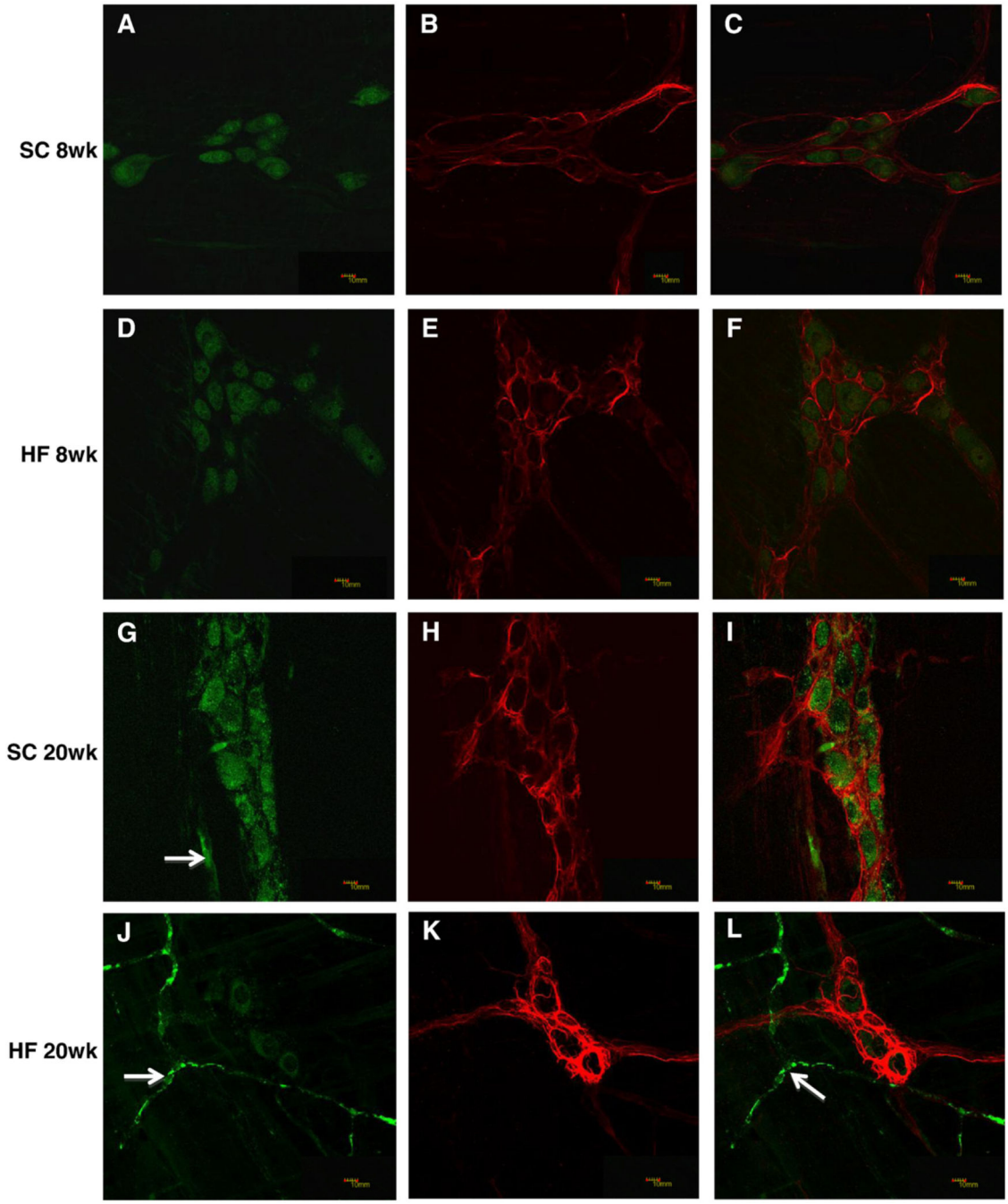

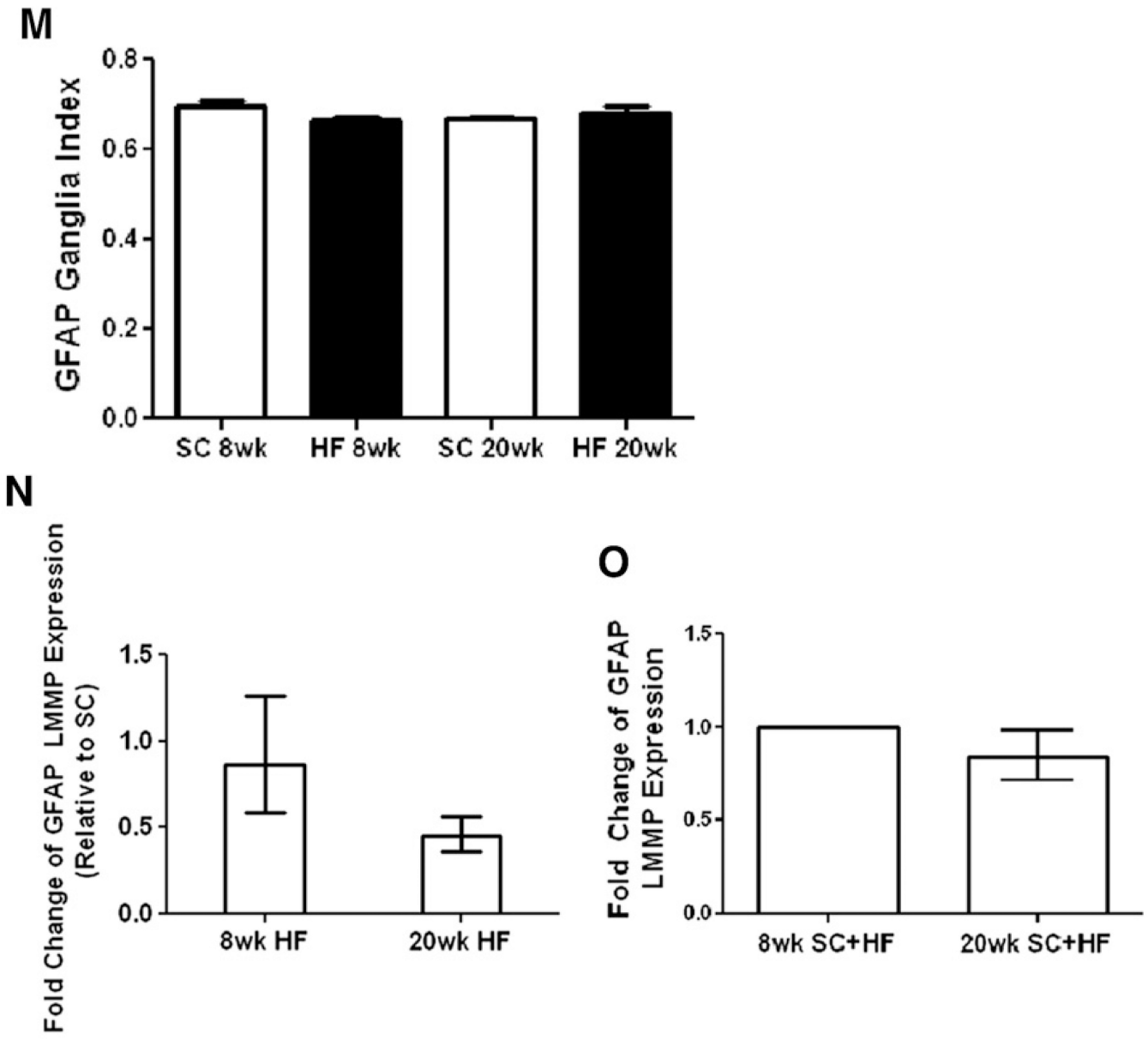

Fig. 3.

Glial fibrillary acidic protein density index and expression were unchanged in the myenteric plexus of HF diet-fed mice. Duodenal LMMP preparations from SC (8 weeks; A–C, 20 weeks; G–H) and HF (8 weeks; D–F, 20 weeks; J–L) diet mice were stained with both HuC/HuD (A, D, G, J) and GFAP (B, E, H, K) antibodies and merged for analysis (C, F, I, L). Arrows in G, J and L show non-specific staining of blood vessels by the Donkey anti Mouse DyLight 488 secondary antibody. The density index (stained area/total ganglia area) of GFAP did not change based on diet or age (M; n = 5–7). Expression levels of GFAP are also not significantly different in mice based on diet (N; n = 4–6) or age (O; n = 4).

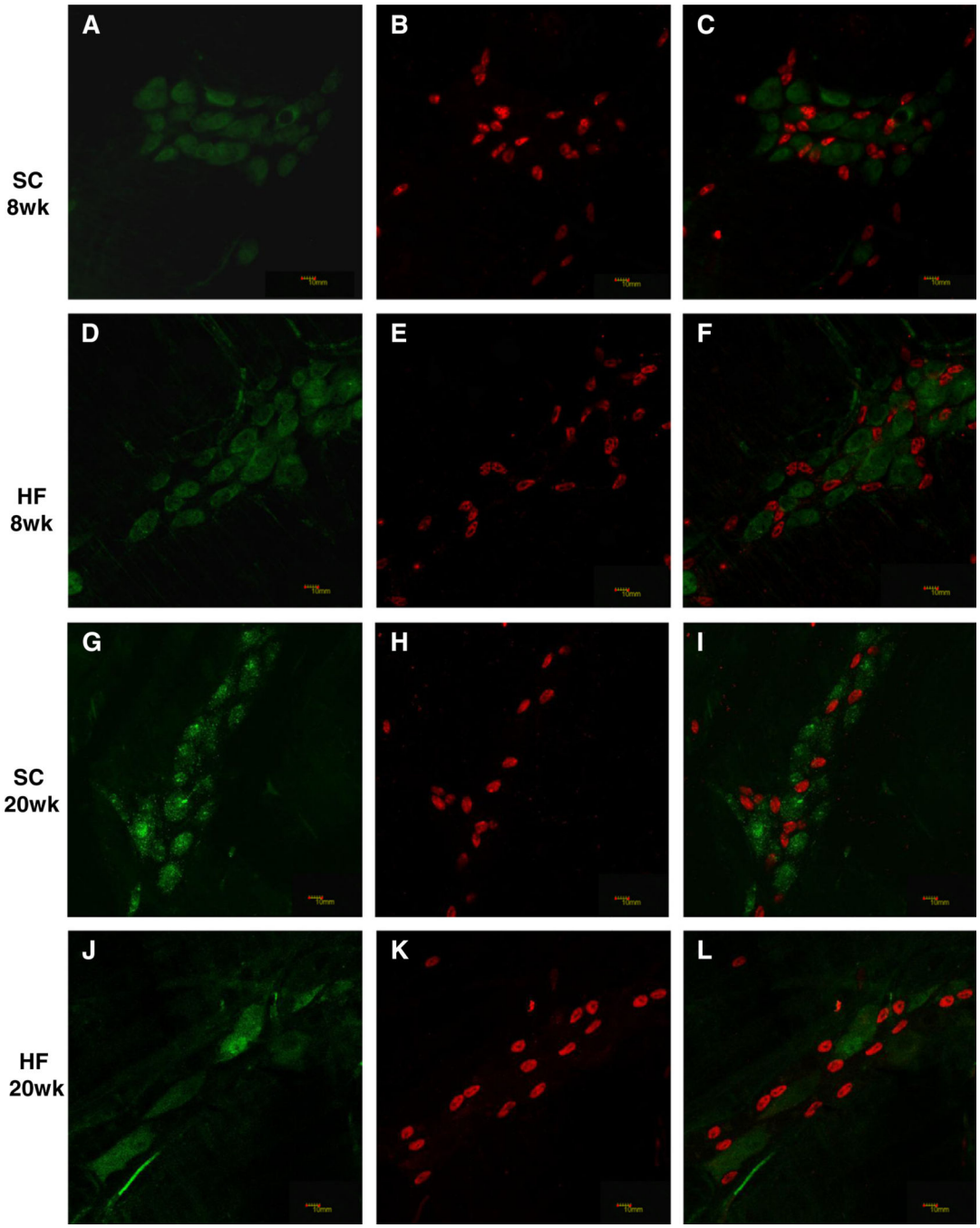

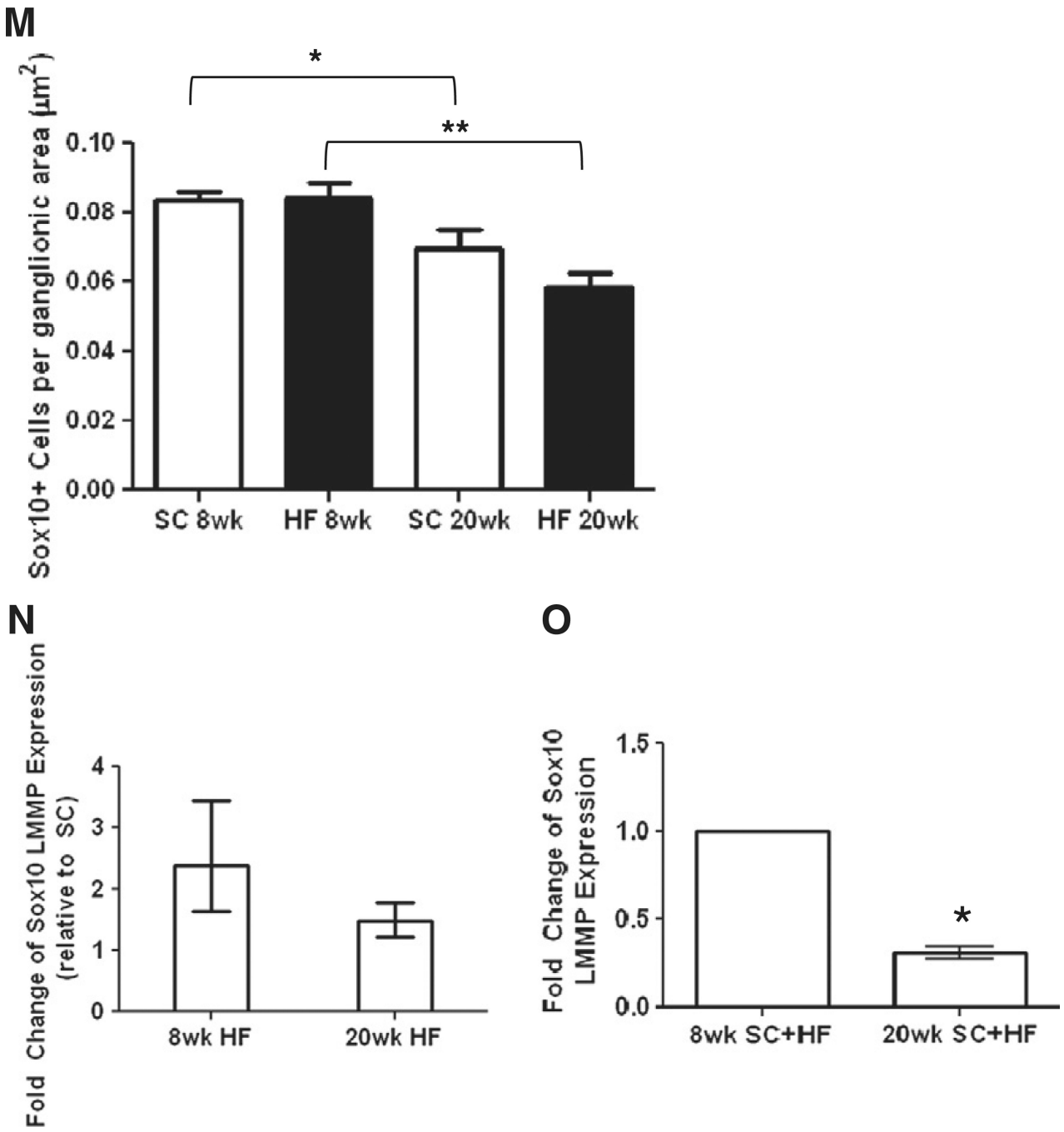

Fig. 4.

Sox10 expression and immunostained EGCs in LMMP decline with mouse age. SC (8 weeks; A–C, 20 weeks; G–I) and HF (8 weeks; D–F, 20 weeks; J–L) duodenal LMMP preparations were stained with HuC/HuD (A, D, G, J) and Sox10 (B, E, H, K) antibodies and merged for analysis (C, F, I, L). Number of Sox10 labeled cells declined with mouse age (M; SC, n = 5–6, *P < 0.05; HF, n = 5–6, **P < 0.01; unpaired students *t*-test) but did not decline due to HF diet. Meanwhile, expression levels of Sox10 did not change based on

HF diet (N; n = 4–6) but declined due to mouse age as well (O; n = 4, *P < 0.05, mixed linear regression).

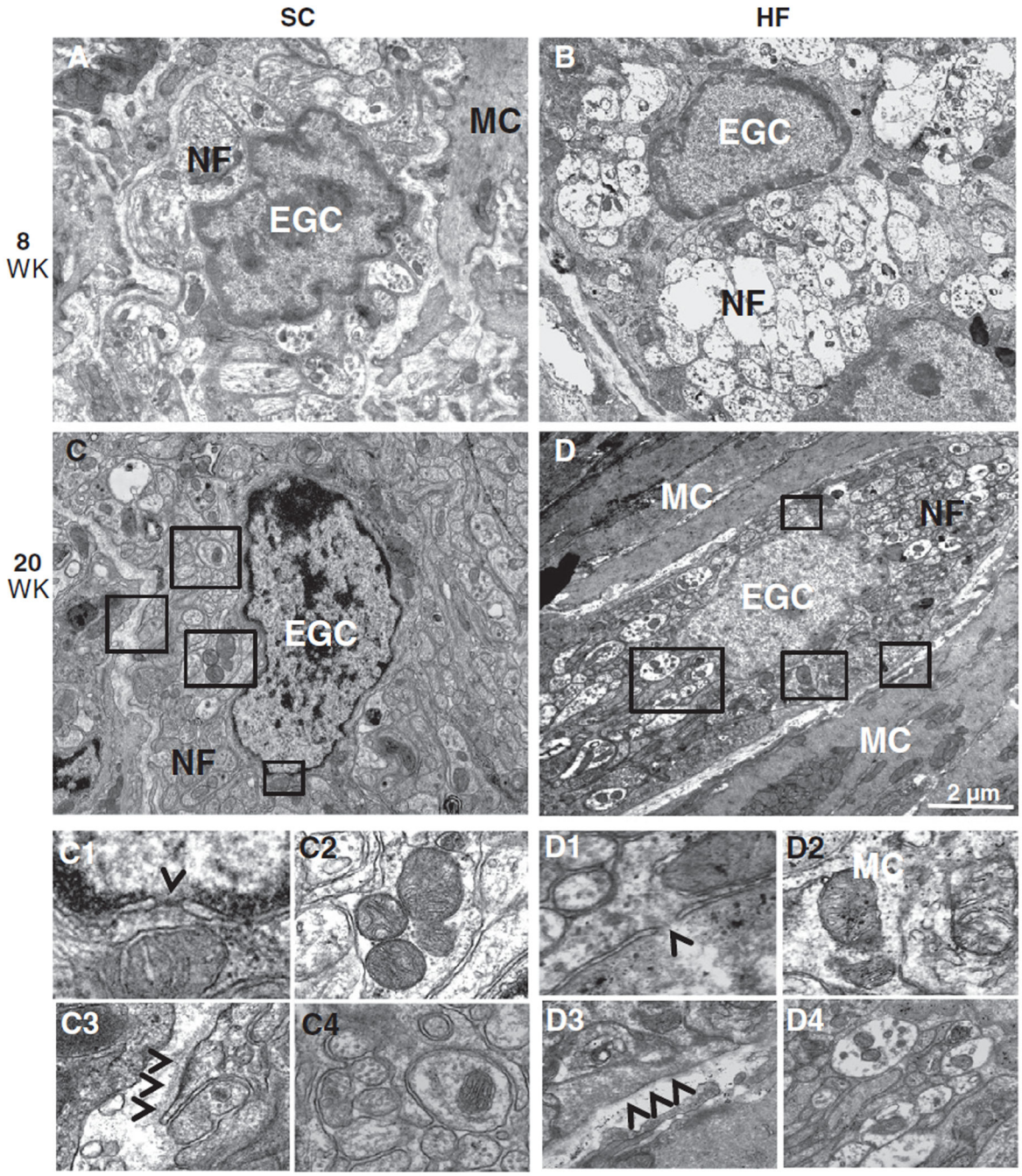

Fig. 5.

TEM analysis of EGCs in the myenteric plexus did not show differences between SC and HF mice. Ultrastructural analysis of EGCs revealed normal morphology in SC (A, C) and HF (B, D) mice at 8 and 20 weeks. Inserts show karyolemm and nuclear pores with no signs of rupture or apoptosis (arrowhead: C1 and D1), healthy mitochondria (C2 and D2) and no signs of basement membrane thickening (arrowheads: C3 and D3) around EGCs of each mouse group. This is regardless of the early signs of neuropathy (axonal edema and loss of

neurofilaments) seen in unmyelinated nerve fibers (NF) of HF (D4) but not SC (C4) mice. Muscle cells (MC) are also seen and exhibit normal morphology.

Table 1

Antibody and manufacturer information for immunohistochemistry.

Tissue	Primary antibody, dilution	Secondary antibody, dilution	Dye, dilution
LMMP	Ms monoclonal neuronal HuC/D, 1:200	Dk anti Ms IgG Dylight 488, 1:300	NA
	Molecular Probes, Eugene, OR A21271	Jackson ImmunoResearch, West Grove, PA 715-485-150	
LMMP	Chk polyclonal GFAP, 1:1000	Dk anti Chk IgY Dylight 594, 1:300	NA
	Abcam, Cambridge, MA ab4674	Jackson ImmunoResearch, West Grove, PA 703-515-155	
LMMP	Gt polyclonal Sox10, 1:150	Dk anti Gt IgG Dylight 594, 1:300	NA
	SantaCruz Biotechnology, Santa Cruz, CA sc-17342	Jackson ImmunoResearch, West Grove, PA 705-515-003	
M	Rb polyclonal S100 protein, 1:400	Biotinylated Gt anti Rb IgG, 1:300	Streptavidin Cy3 conjugate, 1:600
	DakoCytomatio, Glostrup Denmark Z0311	Vector Labs, Burlingame, CA BA 1000	Life Technologies, Grand Island, NY SA1010

LMMP: longitudinal muscle myenteric plexus preparation; M: full-thickness cryostat sections; Rb: Rabbit; Gt: Goat; Ms: Mouse; Dk: Donkey; Chk: Chicken.